Enhancing Length Extrapolation in Sequential Models with Pointer-Augmented Neural Memory

Anonymous authors
Paper under double-blind review

Abstract

We propose a solution called Pointer-Augmented Neural Memory (PANM) to help neural networks understand and apply symbol processing to new, longer sequences of data. PANM integrates an external neural memory that uses physical addresses and pointer manipulation techniques to mimic human and computer symbol processing abilities. PANM facilitates pointer assignment, dereference, and arithmetic by explicitly using pointers to access memory content. Remarkably, it can learn to perform these operations through end-to-end training on sequence data, powering various sequential models. Our experiments demonstrate PANM's exceptional length extrapolating capabilities and improved performance in tasks that require symbol processing, such as algorithmic reasoning and Dyck language recognition. Additionally, PANM helps Transformer achieve up to 100% generalization accuracy in compositional learning tasks and significantly better results in mathematical reasoning, question answering and machine translation tasks.

1 Introduction

Systematic generalization underpins intelligence, and it relies on the ability to recognize abstract rules, extrapolating them to novel contexts that are distinct yet semantically similar to the seen data. Current neural networks or statistical machine learning fall short of handling novel data generated by symbolic rules even though they have achieved state-of-the-art results in various domains. Some approaches can show decent generalization for single or set input data (Bahdanau et al., 2018; Gao et al., 2020; Webb et al., 2020). Yet, neural networks in general still fail in sequential symbol processing tasks, even with slight novelty during inference (Lake and Baroni, 2018; Delétang et al., 2022). For instance, these models can easily learn to duplicate sequences of 10 items, but they will fail to copy sequences of 20 items if they were not part of the training data. These models overfit the training data and perform poorly on out-of-distribution samples such as sequences of greater length or sequences with novel compositions. The issue also affects big models like Large Language Models, making them struggle with symbolic manipulation tasks (Qian et al., 2023). *This indicates that current methods lack a principled mechanism for systematic generalization.*

From a neuroscience perspective, it has been suggested that the brain can execute symbol processing through variable binding and neural pointers, wherein the sensory data are conceptualized into symbols that can be assigned arbitrary values (Kriete et al., 2013). Like the brain, computer programs excel at symbolic computations. Programmers use address pointers to dynamically access data or programs, and have flexible control over the variable. Their programs can work appropriately with unseen inputs.

Building on these insights, we propose a pointer-based mechanism to enhance generalization to unseen length in sequence prediction, which is a crucial problem that unifies all computable problems (Solomonoff, 2010). *Our mechanism is based on two principles:* **(I)** explicitly modeling pointers as physical addresses, and **(II)** strictly isolating pointer manipulation from input data. As such, we need to design a memory that supports physical pointers, and create a model that manipulates the pointers to perform abstract rules and

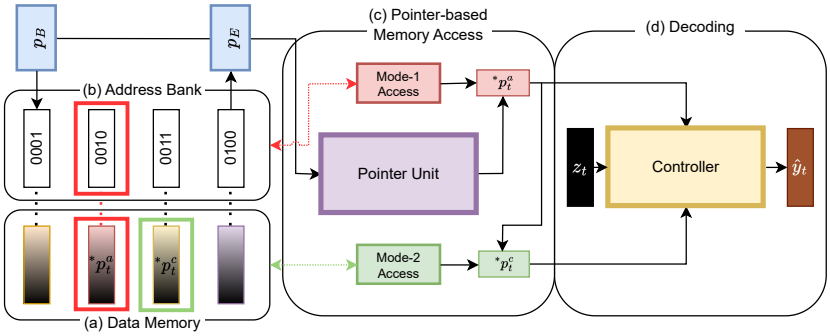

Figure 1: PANM architecture. (a) The data memory contains the encoded input sequence (b) The address bank contains physical addresses associated with data memory slots. The base and end addresses (p_B, p_E) define the address range of the input sequence. (c) The Pointer Unit takes p_B, p_E, recurrently generates the current pointer p_t^a and gets its value $^*p_t^a$ via Mode-1 (red)/2 (green) Access. (d) The Controller takes pointer information, decoding input ($z_t = y_{t-}$), and produce the t-th output token $\hat{y}_t$.

access to the memory. Our memory, dubbed Pointer-Augmented Neural Memory (PANM), is like RAM in Von Neumann architecture (Von Neumann, 1993), which is slot-based, and each memory slot consists of two components: data and address. Unlike initial endeavors that implicitly model pointers as attention softmax (Vinyals et al., 2015; Kurach et al., 2015), our addresses are generated to explicitly simulate physical memory addresses, i.e., incremental binary numbers, which is critical for generalization to longer sequences.

To manipulate a pointer, we create an address bank that contains physical addresses corresponding to the input sequence, and use a neural network called Pointer Unit that is responsible for transforming pointers from an initial address in the address bank. Through attention to the address bank, a new pointer is generated as a mixture of the physical addresses, which can point to different memory slots to follow the logic of the task. We aim to let the Pointer Unit learn the symbolic rules of the task in an end-to-end manner. Finally, given a (manipulated) pointer, the model can access the data through 2 modes of pointer-based access: pointer dereference (Mode-1) and relational access (Mode-2). Our memory can be plugged into common encoder-decoder backbones such as LSTM or Transformer.

Our contribution is a novel memory architecture that incorporates explicit pointer and symbol processing, working seamlessly with sequential models to generalize better. We examine our model in symbol-processing domains such as algorithms and context-free grammar where PANM effectively works with LSTM and StackRNN. We apply PANM to improve the generalization of Transformer models on compositional learning, using SCAN and mathematics datasets. Also, we observe PANM's superior performance in more realistic question answering and machine translation tasks. Our focus is not on striving for state-of-the-art results requiring specialized designs tailored to specific tasks. Our objective is to highlight the generalization improvement achieved by integrating our memory module into fundamental sequential models, with minimal architectural changes, and *showcase the importance of using fundamental generalizing principles to address limitations of current deep learning.*

2 Methods

2.1 Problem Formulation

In sequence-to-sequence (s2s) problems, each data point is an input sequence $X_i = \{x_t^i\}_{t=1}^{l(X_i)}$, associated with a target sequence $Y_i = \{y_t^i\}_{t=1}^{l(Y_i)}$ where l is a function returning the length of the sequence. A model Φ takes the input X_i and generates an output sequence $\hat{Y}_i = \{\hat{y}_t^i\}_{t=1}^{l(\hat{Y}_i)}$ where the predicted sequence terminates as the model outputs a special token $\hat{y}_{t=l(\hat{Y}_i)}^i =$

$<$ eos $>$. Each predicted token is sampled from a categorical distribution, parameterized by Φ and conditioned on the input sequence and optionally with previous output tokens: $\hat{y}_t^i \sim p_\Phi(y_t|X_i, y_{t-}^i)$ where y_{t-}^i can be $\{y_k^i\}_{k=1}^{t-1}$ (true outputs) or $\{\hat{y}_k^i\}_{k=1}^{t-1}$ (predicted outputs) or even zero, depending on the setting (training or inference). We train Φ by minimizing the following cross-entropy loss: $\mathcal{L} = \mathbb{E}_i \left[-\sum_t \log p_\Phi(y_t^i|X_i, y_{t-}^i)\right]$. We are interested in the ability to handle inputs of arbitrary length, so we focus on settings in which the length of testing input sequences is larger than that of training ones: $\max l(X_i) < \min l(X_j)$ with $X_i \in \mathcal{D}_{train}$ and $X_j \in \mathcal{D}_{test}$. In the following sections, when there is no confusion, we will drop the sample index i or j for ease of reading. We note that autoregression is a special case of the s2s formulation where the input and output are from the same domain, and the target sequence is one step ahead of the input sequence.

2.2 Pointer Modeling

Computers are powerful thanks to their ability to manipulate pointers. These pointers store the address of data in memory. Following ***C*** programming language notation, let p denote a pointer associated with a data d in memory $\mathtt{M}$, then p is also the address of the memory slot containing d, i.e., $p = \&d$. We can access the data via p as $^*p = d$, which is also known as *pointer dereference*. We can manipulate the pointer to execute various tasks. For example, if the task is to copy the list X to a new list Y, repeating this simple pointer-based procedure performs correctly regardless of the list length and the values in X: $^*\&Y = {}^*\&X; \&Y = \&Y + 1; \&X = \&X + 1$.

In this paper, we propose a way to model pointers by constructing a bank of addresses, analogous to the addresses in computer architecture. The address bank starts with a *base address* p_B and increases to form an arithmetic sequence with the common difference of 1. For example, if the bank has 3 addresses and $p_B = 3$, the addresses are $\mathtt{A} = \{3, 4, 5\}$. We represent the address as b-bit binary vectors, so we have $\mathtt{A} = \{0010, 0011, 0100\}$ when $b = 4$. The address space is 2^b b-bit binary vectors. Given a memory $\mathtt{M}$ containing $l(\mathtt{M})$ slots, we bind each slot to an address in the address bank $\mathtt{A}$ such that $\mathtt{A}[t] = \&\mathtt{M}[t]$ and $^*\mathtt{A}[t] = \mathtt{M}[t]$ $(1 \leq t \leq l(\mathtt{M}))$. We use p_E as the *end address* to refer to the final address corresponding to the last item in $\mathtt{M}$.

The memory $\mathtt{M}$ stores the input sequence, and its size depends on the input length: $l(\mathtt{M}) = l(X)$. To enable generalization, the address space should cover a wide range of addresses that is greater than the sequence length range (i.e., $2^b > \max l(X)$). More importantly, during training, all possible addresses should be exposed to the model. Otherwise, any unexposed address will confuse the model when it appears during inference. As such, during training, we *uniformly sample the base address* p_B from the address space to construct the address bank $\mathtt{A}$ for each sequence memory $\mathtt{M}$. This ensures any address in the address space will eventually appear between the base and end addresses. See Appendix B for an illustrative example of the base address sampling mechanism and its complexity.

Given the address bank, we can perform pointer-based procedures to achieve generalization. To do so, we need pointer variables p_t denoting pointers used by the model at timestep t. As for the copy task, the model outputs correctly by accessing and manipulating the pointer variables through 3 important pointer operations: $p_t = \mathtt{A}[t]$ (*assignment*); $\hat{y}_t^i = {}^*p_t$ (*dereference*); $p_t = p_t + 1$ (*arithmetic*), which will be described in the next section.

2.3 Pointer-Augmented Neural Memory (PANM)

PANM acts as an external memory module for any neural network to support it handling sequence data. In such a memory-augmented neural network, a neural Controller ($\mathtt{Ctrl}$) interacts with the memory ($\mathtt{M}$) to read/write data and make predictions on the output target. Unlike traditional neural memory, PANM is equipped with an address bank ($\mathtt{A}$) and a Pointer Unit ($\mathtt{PU}$) to support pointer operations. To simplify memory writing operations, PANM transforms the whole input sequence X to the memory $\mathtt{M}$ in the encoding phase such that $L = l(\mathtt{M}) = l(X)$ using $\mathtt{M} = \mathtt{Encoder}_\theta(X)$ where $X \in \mathbb{R}^{d_x \times L}$, $\mathtt{M} \in \mathbb{R}^{d_m \times L}$ and the $\mathtt{Encoder}$, parameterized by θ, can be any neural encoder such as LSTM or Transformer.

The address bank $\mathtt{A} \in \{0,1\}^{b \times L}$ is then created and bound to $\mathtt{M}$ as mentioned in the previous section. During decoding, the encoded information in $\mathtt{M}$ is not changed and the controller focuses only on reading from $\mathtt{M}$ to produce the right output sequence. An overview of PANM decoding process is given in Fig. 1.

2.3.1 Pointer Unit

At each timestep t of the decoding process, PANM makes use of pointer variables p_t^a, which are initialized as a valid address in the address space and then updated by the Pointer Unit $\mathtt{PU}$. In particular, the $\mathtt{PU}$, implemented as an GRU (Chung et al., 2014), takes an address from $\mathtt{A}$ as its initial inputs, e.g., $p_0^a = p_B$, and recurrently produces a key h_t^a that performs *address attention* to create succeeding pointer variables p_t^a:

$$h_t^a = \mathtt{GRU}_\varphi\left(p_{t-1}^a, h_{t-1}^a\right); w_t^a\left[n\right] = \text{softmax}\left(\frac{h_t^a g_\varphi^a\left(\mathtt{A}[n]\right)}{\left\|h_t^a\right\| \left\|g_\varphi^a\left(\mathtt{A}[n]\right)\right\|}\right); p_t^a = \mathtt{A} w_t^a \tag{1}$$

where h_0^a is initialized as 0 and $1 \leq n \leq l(X)$, φ denotes the parameter of the $\mathtt{PU}$ and $g^a(\cdot)$ is a feed-forward neural network to transform the address to the same space as h_t^a. According to § 1's principle **I**, p_t^a is "softly" *assigned* a physical address value in the address bank. Our pointer, p_t^a, offers several advantages over "implicit pointers" made up of the attention weights (w_t^a), which are commonly utilized in previous works (Vinyals et al., 2015; Luong et al., 2015). First, p_t^a is a combination of physical addresses represented by binary numbers, and therefore its dimension is generally independent of the sequence length. In contrast, the dimension of w_t^a varies with the input length. Therefore, arithmetic transformations on p_t^a are easier than on w_t^a. Second, longer testing length poses challenges for traditional attentions to accurately produce w_t^a pointing to unseen location. Using "physical key" A to compute w_t^a mitigates this issue by employing random physical address ranges (see § 2.2).

Following § 1's principle **II**, the $\mathtt{PU}$ *recurrently transforms* the original p_0^a to a series of pointers $\{p_t^a\}_{t=1}^{l(\hat{Y})}$ suitable for the current task *without using input data*. This prevents unseen testing inputs disturb $\mathtt{PU}$'s transformations. In the copy example, an ideal arithmetic transformation ensure $p_0^a = p_B$ and $p_{t+1}^a = p_t^a + 1$, which performs perfectly for any sequence whose length $\leq 2^b$. We aim to learn $\mathtt{PU}$ to automatically discover pointer manipulation rules from the task. As the rules are learned, generalization is achieved even when the testing sequence is longer or contains novel items.

2.3.2 Pointer-based Addressing Modes

Mode 1 In this mode, the content from memory $\mathtt{M}$ is retrieved directly by dereferencing pointers. To *dereference* pointer p_t^a, we utilize the $\mathtt{A} - \mathtt{M}$ binding and the address attention weight w_t^a, retrieving the pointer value associated with p_t^a as ${}^*p_t^a = \mathtt{M} w_t^a$. Through this dereference operator, we can access to arbitrary data in the memory $\mathtt{M}$ without relying on the content of the memory. This property enables robustness in handling new sequence when the memory content is novel and the process stays the same (e.g., copy a never-seen-before sequence). Accessing $\mathtt{M}$ indirectly via $\mathtt{A}$ allows more memory slots to be added to $\mathtt{M}$ during inference without affecting the processing rule as long as the $\mathtt{PU}$ can transform the pointer variable correctly. During training, $\mathtt{PU}$ experiences pointer variables covering the whole address space because the base address is sampled randomly. Hence, it is possible for $\mathtt{PU}$ to correctly transform pointers that point to extended addresses of a growing memory as long as the pointer manipulation rule does not change. The address attention can be used for multiple pointer variables. In this case, there would be multiple pointer units $\{\mathtt{PU}_h\}_{h=1}^{H^a}$ responsible for several $\left\{p_{t,h}^a\right\}_{h=1}^{H^a}$ and $\left\{{}^*p_{t,h}^a\right\}_{h=1}^{H^a}$ where H^a is the number of attention heads. These pointer values will be used by the Controller for other memory reading.

Mode 2 This mode uses a more complicated memory access mechanism to capture relations between pointers in complicated reasoning tasks. *The accessed content is not the one associated with the current pointer*, but those whose contents are related to the current pointer's

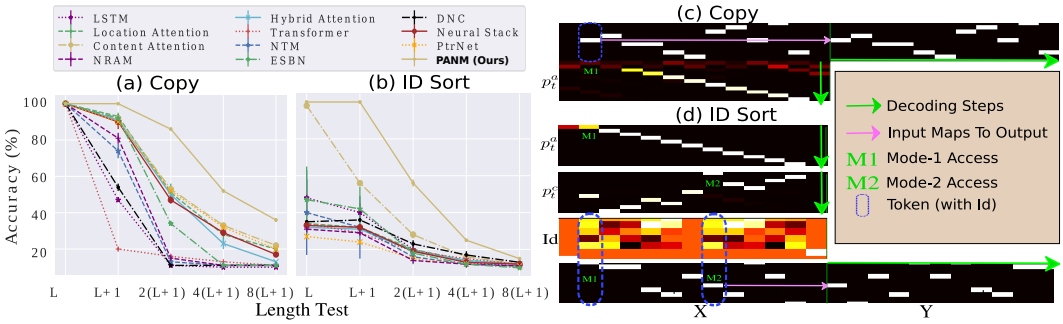

Figure 2: Exemplar results on 2 algorithms. (a, b) Test accuracy (mean ± std) over 5 runs on Copy and ID Sort on each length test, respectively. Random predictor would reach around 10% accuracy. (c,d) Visualization of data and pointer's slots for Copy and ID Sort, respectively.

value. As an example, selection sort algorithm may require comparing items in a list with the Mode-1 pointer's item to select the greater one. We simulate that using attention with the query as the current pointer value:

$$q_t = g^c_\varphi\left(\left\{{}^*p^a_{t,h}\right\}_{h=1}^{H^a}\right); w^c_t[n] = \text{softmax}\left(\frac{q_t \mathtt{M}[n]}{\|q_t\| \, \|\mathtt{M}[n]\|}\right); {}^*p^c_t = \mathtt{M} w^c_t \tag{2}$$

Here, the pointer attention takes the concatenated values $\left\{{}^*p^a_{t,h}\right\}_{h=1}^{H^a}$ as input, transforms them to a query q_t using a feed-forward neural network $g^c(\cdot)$, and returns the related pointer value ${}^*p^c_t$ through attention mechanisms on $\mathtt{M}$. Intuitively, the Pointer Unit manipulates the Mode-1 pointer p^a_t such that it retrieves the desired content pointed by the Mode-2 pointer p^c_t. We can also have multi-head attention, which results in $\left\{{}^*p^c_{t,h}\right\}_{h=1}^{H^c}$ where H^c is the number of attention heads.

2.3.3 The Controller

The Controller `Ctrl` is responsible for decoding the memory to produce outputs. Unlike other methods, we have pointer-based memory access to provide the controller with symbol-processing information. In particular, at the t-th step of the decoding, `Ctrl` takes the pointer values (mode 1 and 2) as input together with an optional decoding input ($z_t = y_{t-}$), and uses a GRU to recurrently produce the hidden state h^c_t as follows,

$$h^c_t = \mathtt{GRU}_\lambda\left(\left[\left\{{}^*p^a_{t,h}\right\}_{h=1}^{H_a}, \left\{{}^*p^c_{t,h}\right\}_{h=1}^{H_c}, z_t\right], h^c_{t-1}\right) \tag{3}$$

where the hidden state h^c_0 is initialized as $\sum_i \mathtt{M}[i]$ and λ is the parameters of `Ctrl`. The `GRU` handles content-based input, empowered with pointer information to construct rich hidden state representations. Furthermore, the pointer-based data give the `GRU` access to correct items in the sequence even when the memory content becomes different from the training due to encountering novel sequence length.

The Controller `Ctrl` uses the pointer values (mode 1), the related pointer values (mode 2) and the hidden state h^c_t to make the final prediction. It simply concatenates them and forward to the $g^o(\cdot)$–a MLP, to generate the output token $\hat{y}^i_t \sim p_\Phi(y_t|X_i, z_t) = g^o_\lambda\left(\left[\left\{{}^*p^a_{t,h}\right\}_{h=1}^{H^a}, \left\{{}^*p^c_{t,h}\right\}_{h=1}^{H^c}, h^c_t\right]\right)$. The pointer values allow g^o to fully utilize pointer information in producing the final output. Φ consists of the parameters of the $\mathtt{Encoder}_\theta$, Pointer Unit $\mathtt{PU}_\varphi$ and Controller $\mathtt{Ctrl}_\lambda$. `Ctrl` can be put on top of another decoder to process the decoding input z_t. In some experiments, we use Transformer as the decoder (see Appendix C and D.3). A summary of PANM's operation is given in Algo. 1 in Appendix.

Task	Copy	Reverse	Mix	D. Recall	P. Sort	ID Sort
Other Max	60.2	63.6	64.0	47.6	60.6	42.1
PANM (Ours)	**74.8**	**73.6**	**81.2**	**52.8**	**67.8**	**59.2**

Table 1: Algorithmic reasoning: mean sequence-level accuracy (%) over testing lengths Other Max is selected as the best numbers at each length mode from other baselines.

3 Experimental Results

In our experiments, we use two pointer variables in Mode-1 access and one for Mode-2 to balance between performance and computing cost ($H^a = 2$, $H^c = 1$, see more in Appendix C). The two Mode-1 pointer variables are initialized as the base and end addresses. All MLPs in PANM have 1 hidden layer of 128 dimensions. We use 256-dimensional GRUs for `PU` and `Ctrl`. The memory's address space has $b = 10$ bits, corresponding to a maximum of 1024 unique addresses, which is greater than any sequence length in the experiments.

In §3.1-3.3, our chosen tasks are representative of various types of symbolic reasoning and well-known benchmarks to measure the symbol-processing capability of ML models. *To showcase that these tasks are non-trivial, we report how Chat-GPT failed on our tasks in Appendix* D.6. We validate the contribution of our methods in other practical tasks in §3.4. We also explain the choice of competing baselines in Appendix D.

3.1 Algorithmic Reasoning

In our first experiment, we study the class of symbol processing problems where an output sequence is generated by a predefined algorithm applied to any input sequence (e.g., copy and sort). The tokens in the sequences are symbols from 0 to 9. The input tokens can be coupled with meta information related to the task such as the priority score in Priority Sort task. During training, the input sequences have length up to L tokens and can grow to $L + 1$, $2(L + 1)$, $4(L + 1)$ or $8(L + 1)$ during testing. Our setting is more challenging than previous generalization tests on algorithmic reasoning because of four reasons: (1) the task is 10-class classification, harder than binary prediction in Graves et al. (2014), (2) the testing data can be eight time longer than the training and the training length is limited to $L \approx 10$, which is harder than Grefenstette et al. (2015), (3) there is no curriculum learning as in Kurach et al. (2015), and (4) the training label is the one-hot value of the token, which can be confusing in case one token appears multiple times in the input sequence and tougher than using label as the index/location of the token as in Vinyals et al. (2015).

Here, we design several tasks**.** **Content-free tasks** involve permuting tokens in input sequence using certain position-based rules: First-In-First-Out (*Copy*), Last-In-First-Out (*Reverse*) and *Mix*. While the first two rules demand linear pointer manipulations (traverse the sequence from the head or tail, to output the target token), the last one uses a non-linear, length-dependent manipulation rule: if t is odd, $y_t = x_{\lceil \frac{L}{2} \rceil}$; if t is even, $y_t = x_1$. **Content-based tasks** need the input's token value together with symbol processing to arrange the output sequence. We introduce 3 tasks: *Dynamic Recall*, *Priority Sort* and *ID Sort*. Readers can find the details of these tasks in Appendix D.1.

Baselines are categorized into 4 groups: (1) Traditional RNNs such as LSTM (Hochreiter and Schmidhuber, 1997), (2) Sequential attention models: Content Attention (Bahdanau et al., 2014), Location Attention (Luong et al., 2015), Hybrid Attention (our baseline concatenates the attention vectors from content and location attention), (3) MANNs such as NTM (Graves et al., 2014), DNC (Graves et al., 2016), Neural Stack (Grefenstette et al., 2015) and Transformer (Vaswani et al., 2017), and (4) pointer-aware models: NRAM (Kurach et al., 2015), PtrNet (Vinyals et al., 2015), ESBN (Webb et al., 2020) and our method PANM. In this synthetic experiment, we adopt LSTM as the encoder for PANM. All baselines are trained with fixed number of steps (100K for ID Sort and 50K for the rest), which is enough for the training loss to converge. For each task, each baseline is trained 5 times with different random seeds and we use the best checkpoint on $L + 1$ mode validation to evaluate the baselines.

Task	SCAN (L cut-off)											Math	
	22	24	25	26	27	28	30	32	33	36	40	a.s	p.v
U. TRM+RPE	20	12	71	**100**	**100**	**100**	**100**	**100**	**100**	**100**	**100**	**97**	75
TRM+RPE	20	12	31	61	**100**	**100**	**100**	94	**100**	**100**	**100**	91	0
U. TRM	2	5	14	21	26	0	6	35	0	0	0	94	20
TRM	0	4	19	29	30	8	24	36	0	0	0	89	12
PANM (Ours)	**22**	**47**	**100**	**100**	**100**	**100**	**100**	**100**	**100**	**100**	**100**	**97**	**86**

Table 2: SCAN (Left): Exact match accuracy (%, median of 5 runs) on splits of various lengths. Mathematics (Right): mean accuracy over 5 runs. The baselines' numbers are from Csordás et al. (2021) and we run PANM using the authors' codebase.

Results We report the average accuracy across different testing length for each task in Table 1. Overall, PANM significantly outperforms the best competitors ranging from 10-20% per task. Compared with individual baselines, the improvement is much higher (Appendix D.1). We illustrate how the pointer manipulation works for Copy and ID Sort in Fig. 2c and d. In Copy, only Mode-1 access is needed. As decoding step t increases, Pointer Unit generates p_t^a following the increment of the addresses as expected. In ID Sort, both Mode-1 and 2 are needed. The Pointer Unit generates p_t^a incrementally to trace the input tokens from left to right (Mode 1). Then, the Mode-2 pointer p_t^c is computed via attention to discover token with the same id, which will be the output at step t. Without Mode-2 access, PANM certainly fails this task. Experiments with varied number of heads are in Appendix D.5.

3.2 Dyck Language Recognition

Truly understanding the hidden law of context-free grammars such as Dyck ($\mathcal{D}_n$) is challenging for neural networks, even those with memory and attention (Yu et al., 2019). The language consists of strings with balanced pairs of brackets of different types ($|_1, |_2, ..., |_n$), generated by the following rules: $S \rightarrow |_i S|_i$ with probability p/n or SS with probability q or ϵ with probability $1 - p - q$. Here, p, q are parameter of the language and ϵ is equivalent to EOS token. We follow the sequence prediction task and datasets in Suzgun et al. (2019) where the input is an unfinished Dyck string, and the output is the set of possible brackets for the next token, e.g., for $\mathcal{D}_2$, ([] $\rightarrow$ (or) or [. We follow the authors to enable set prediction by representing output y_t as a multi-hot vector.

We adapt PANM to this autoregression task by masking `M` to ensure the decoder only see tokens up to the current decoding step. Since the token set is simple, we do not need to use any encoder, i.e., raw input tokens are stored in `M`. The SOTA baseline in this task is SRNN (Suzgun et al., 2019), an autoregressive model using stack as memory. We use this model as the decoder to make the setup of PANM close to SRNN. The only difference is that PANM has Pointer-Based Memory Access (Fig. 1b). To make the task more challenging, we limit the maximum training length L to 10 ($\mathcal{D}_2$) and 20 ($\mathcal{D}_3$) tokens, and the testing lengths are $L + 2$, $2L$, $4L$, $8L$. We choose L as minimum numbers such that the model can perform decently on training data. The standard training and testing sizes are 5000. We train the models for 5 epochs and evaluate them on the training data at the end of each epoch to save model checkpoints. We use the best checkpoints for generalization test.

Fig. 4 (left) in Appendix D.2 reports the models' accuracy for $\mathcal{D}_2$ and $\mathcal{D}_3$. Under our extreme setting, SRNN generalization fades out quickly as test lengths increase, especially for $\mathcal{D}_3$ whereas PANM performance degradation happens at a much slower rate, outperforming SRNN by around 20% on average in both tasks at any test lengths.

3.3 Compositional Learning

SCAN In this task , one needs to map an input sentence into an output sequence of commands (Lake and Baroni, 2018). The sequences are compositional, consisting of reusable parts. For example, in one case, "`jump twice`" should be mapped to "`JUMP JUMP`" and in another, "`walk twice`" becomes "`WALK WALK`". We focus on the "length split" datasets where the training sequences are shorter than the test ones with 11 length modes $L = 22, 24, .., 40$

(Newman et al., 2020). We adopt the benchmark, training procedure and baselines prepared by Csordás et al. (2021), which achieves strong results under standard s2s learning. Here, our aim is not to break SOTA, which can be achieve by hybrid-symbolic architectures (Chen et al., 2020; Shaw et al., 2021). Instead, we focus on improving Transformer generalization in this task, hence the baselines are chosen as several variants of Transformers (TRM) targeted to sequence extrapolation, including those using Relative Positional Encoding (RPE (Dai et al., 2019)) and Universal Transformer (U. TRM (Dehghani et al., 2018)), which is an advanced Transformer variant that recurrently processes each token, and can dynamically adjust the number of processing steps. Following Csordás et al. (2021), each baseline is trained 5 times for 50K steps and the resulting model after training is used for evaluation (no validation). Here, we use Transformer as the `Encoder`, which is the same as the TRM, and stack the Controller to another Transform decoder (see details in Appendix D.3). Hence, the only difference is the decoding where PANM leverages pointer manipulation.

Table 2 shows that PANM outperforms other baselines in the hardest settings when the training length is up-to 22, 24, and 25. For 22 and 24 cases, general models like PANM cannot show perfect generalization because some testing compositions is entirely discarded from the train set. In easier settings, PANM shares the perfect median accuracy with the sophisticated U. TRM + RPE although it does not use RPE. Remarkably, despite sharing the same encoder, TRM performs much worse than PANM and even fails to learn in easy modes (33, 36, 40), indicating the importance of pointer handling in this testbed. One problem for other baselines is the EOS decision (when to generate ending token), which requires length tracking (Newman et al., 2020). As they do not have content-free sequence iteration mechanisms, it is extremely hard to trace the length without overfitting to the training data. On the other hand, PANM can hypothetically generate pointer incrementally and capture the difference between the last and the first pointers, i.e. the input length, and infer the output sequence length based on that information.

Mathematical Problems We also test our model on mathematics (Saxton et al., 2018) where the input/output are questions and answers about math and each token is a character. For example, `What is` $-$ `5` $-$ `110911`? $\rightarrow$ $-$`110916` (add_or_sub) and `What is the hundreds digit of 31253`? $\rightarrow$ `2` (place_value). The task requires not only math reasoning, but also natural language understanding. We follow the training from Csordás et al. (2021) to conduct experiments on 2 subsets: `add_or_sub` (a.s) and `place_value` (p.v), and compare our method with Transformer-based baselines. Here, we focus on the extrapolating test set involving larger numbers, more numbers, more compositions, and thus longer input sequences than the training. In this experiment, we use TRM + RPE as the `Encoder`. The Controller is added to a normal TRM decoder. As shown in Table 2, on `place_value`, PANM does not suffer from performance crash as TRM + RPE (0% test accuracy, as admitted in the paper (Csordás et al., 2021) even though it uses the same encoder). PANM achieves similar results as U. TRM+ RPE on `add_or_sub` while outperforming it by 11% on `place_value`. We also examine PANM with the original Transformer and report additional results in Appendix D.3.

3.4 Other NLP Tasks

Question Answering Our objective is to explore the PANM's generalization beyond obviously compositional data by applying it in a more practical setting of question answering. For this purpose, we utilize two datasets, namely bAbI (Weston et al., 2015) and SQUAD 1.1 (Rajpurkar et al., 2016) where the input sequence is a context paragraph and a question, and the output is the answer. To add complexity to the task, we ensure the length of test sequence is greater than that of the training by sorting the context paragraph by length and splitting the sorted data into 0.8/0.2 and 0.5/0.5 ratio. Details of the data/task are in Appendix D.4. In **bAbI**, we configure the PANM similarly to the one described in § 3.3 using Transformer backbone, and test the models after 100-epoch training. The models predict the answer tokens given the context and question tokens. As shown in Appendix Fig. 4 (right), PANM helps Transformer generalize better, consistently improving around 6% and 5% using 0.8/0.2 and 0.5/0.5 splits, respectively. Notably, PANM's testing loss is not diverged quickly as Transformer's, indicating PANM's capability of reducing overfitting. In **SQUAD**, we use BERT as the backbone to predict the start and the end of the answer

as in Kenton and Toutanova (2019). PANM-assisted model outperforms the baselines by 1% and 2% exact match accuracy, respectively (Appendix Table 13). The improvement is significant as BERT is already pretrained with big data and robust against novel test data.

Machine Translation Here, we want to verify the PANM in machine translation and show that PANM can work with different number layers of Transformer. The results are presented in Appendix Fig 8 where we report the model perplexity on Multi30K (en-de) dataset. The 30K-sample dataset is sorted by input length and split into training and testing s.t. testing sequences are longer, similar to QA task. The results demonstrate PANM can consistently improve the generalization performance of Transformer across different split ratios and the number of encoder/decoder layers.

4 Related works

There are many attempts to augment neural networks with external memory (MANN) to improve their symbol-processing ability. Pioneers such as NTM (Graves et al., 2014) and DNC (Graves et al., 2016) propose computer-like memory read/write operations with content-based attention mechanisms, and thus in principle, can execute any symbolic rules. However, learning the hidden law end-to-end from sequence data is extremely difficult. Therefore, MANNs including Transformers (Vaswani et al., 2017), may fail miserably in out-of-distribution testbeds, especially length extrapolation (Delétang et al., 2022). Recent LLMs are good at reasoning and generalization, but bad at symbolic processing (Qian et al., 2023; Tang et al., 2023). We use LLMs only to show our task difficulty (Appendix D.6), not as a baseline, because they are not on the same scale as our method.

Many recent works advocate the use of specialized memory architectures such as stacks (Grefenstette et al., 2015; Hao et al., 2018; Suzgun et al., 2019), key-value memory (Webb et al., 2020; Le et al., 2020a) and improved attentions (Kurach et al., 2015; Russin et al., 2019; Dubois et al., 2020). These methods employ different inductive biases in designing the memory and attention, *yet not following the two principles advocated by our paper*. Although they may work remarkably on certain synthetic tasks, they are not examined on various benchmarks or compatible with different sequential backbones. Other orthogonal approaches focus on model initialization (Zhang et al., 2019), data augmentation (Andreas, 2020) or training details (Csordás et al., 2021). Besides differentiable models, there are major progress in compositional rule learning that leverage neuro-symbolic architectures (Nye et al., 2020; Shaw et al., 2021; Chen et al., 2020) or reinforcement learning (Liu et al., 2020). We have not compared our model with these task-specific methods, as our focus is on improving the systematic generalization of fundamental differentiable models.

Our approach is mainly related to key-value memory because the address bank can be viewed as the key and the data memory as the value. However, the key in other works is either learned through backpropagation (Le et al., 2020a) or computed based on the input data (Webb et al., 2020). In contrast, our "keys" are generated as fixed numbers (physical memory addresses– § 1's principle **I**), which is totally separated from the data and extendable to longer sequences. We argue that using addresses as keys is critical to symbol processing because it explicitly allows pointer assignment, dereference and arithmetic. A related generalization-enable scheme is to design positional encoding of tokens in a sequence (Vaswani et al., 2017; Dai et al., 2019; Li and McClelland, 2022). Unlike these approaches, our physical addresses are detached from the data to support transforming pointers through time steps and isolating pointer manipulation from the input.

5 Discussion

We introduce a neural memory model called PANM that manipulates pointers to learn symbol processing rules for better length extrapolation. PANM isolates symbols from data and uses an address bank to allow data-isolated pointer manipulation through address attention. PANM consistently outperforms strong baselines in tasks such as algorithm mining, compositional learning, mathematics reasoning, context-free grammar recognition, and practical NLP tasks, even when the test sequence is much longer than the training sequence.

Ethics Statement In this work, we used the publicly available datasets for experiments. We did not collect human or animal data during this study. Our work aims to improve the generalization of sequential models. This aim is genuine, and we do not think there are immediate harmful consequences. However, we are aware of potential problems if our method is used to augment large language models to generate texts that are hallucinated or contain negative contents. This issue is typical for plug-and-play modules like PANM, and we will do our best to prevent it from our end.

Reproducibility Statement In the Appendix, we included our detailed model descriptions, algorithms, implementations, hyperparameters to replicate the results of our experiments. Source code will be released when the paper is published.

References

Jacob Andreas. Good-enough compositional data augmentation. In *Proceedings of the 58th Annual Meeting of the Association for Computational Linguistics*, pages 7556–7566, 2020.

Dzmitry Bahdanau, Kyunghyun Cho, and Yoshua Bengio. Neural machine translation by jointly learning to align and translate. *arXiv preprint arXiv:1409.0473*, 2014.

Dzmitry Bahdanau, Shikhar Murty, Michael Noukhovitch, Thien Huu Nguyen, Harm de Vries, and Aaron Courville. Systematic generalization: What is required and can it be learned? In *International Conference on Learning Representations*, 2018.

Xinyun Chen, Chen Liang, Adams Wei Yu, Dawn Song, and Denny Zhou. Compositional generalization via neural-symbolic stack machines. *Advances in Neural Information Processing Systems*, 33:1690–1701, 2020.

Junyoung Chung, Caglar Gulcehre, KyungHyun Cho, and Yoshua Bengio. Empirical evaluation of gated recurrent neural networks on sequence modeling. *arXiv preprint arXiv:1412.3555*, 2014.

Róbert Csordás, Kazuki Irie, and Jürgen Schmidhuber. The devil is in the detail: Simple tricks improve systematic generalization of transformers. *arXiv preprint arXiv:2108.12284*, 2021.

Zihang Dai, Zhilin Yang, Yiming Yang, Jaime G Carbonell, Quoc Le, and Ruslan Salakhutdinov. Transformer-xl: Attentive language models beyond a fixed-length context. In *Proceedings of the 57th Annual Meeting of the Association for Computational Linguistics*, pages 2978–2988, 2019.

Mostafa Dehghani, Stephan Gouws, Oriol Vinyals, Jakob Uszkoreit, and Lukasz Kaiser. Universal transformers. In *International Conference on Learning Representations*, 2018.

Grégoire Delétang, Anian Ruoss, Jordi Grau-Moya, Tim Genewein, Li Kevin Wenliang, Elliot Catt, Marcus Hutter, Shane Legg, and Pedro A Ortega. Neural networks and the chomsky hierarchy. *arXiv preprint arXiv:2207.02098*, 2022.

Yann Dubois, Gautier Dagan, Dieuwke Hupkes, and Elia Bruni. Location attention for extrapolation to longer sequences. In *Proceedings of the 58th Annual Meeting of the Association for Computational Linguistics*, pages 403–413, 2020.

Aaron Eisermann, Jae Hee Lee, Cornelius Weber, and Stefan Wermter. Generalization in multimodal language learning from simulation. In *2021 International Joint Conference on Neural Networks (IJCNN)*, pages 1–8. IEEE, 2021.

Tong Gao, Qi Huang, and Raymond Mooney. Systematic generalization on gscan with language conditioned embedding. In *Proceedings of the 1st Conference of the Asia-Pacific Chapter of the Association for Computational Linguistics and the 10th International Joint Conference on Natural Language Processing*, pages 491–503, 2020.

Alex Graves, Greg Wayne, and Ivo Danihelka. Neural turing machines. *arXiv preprint arXiv:1410.5401*, 2014.

Alex Graves, Greg Wayne, Malcolm Reynolds, Tim Harley, Ivo Danihelka, Agnieszka Grabska-Barwińska, Sergio Gómez Colmenarejo, Edward Grefenstette, Tiago Ramalho, John Agapiou, et al. Hybrid computing using a neural network with dynamic external memory. *Nature*, 538(7626):471–476, 2016.

Edward Grefenstette, Karl Moritz Hermann, Mustafa Suleyman, and Phil Blunsom. Learning to transduce with unbounded memory. *Advances in neural information processing systems*, 28, 2015.

Yiding Hao, William Merrill, Dana Angluin, Robert Frank, Noah Amsel, Andrew Benz, and Simon Mendelsohn. Context-free transductions with neural stacks. *EMNLP 2018*, page 306, 2018.

Sepp Hochreiter and Jürgen Schmidhuber. Long short-term memory. *Neural computation*, 9(8):1735–1780, 1997.

Jennifer Hu, Jon Gauthier, Peng Qian, Ethan Wilcox, and Roger P Levy. A systematic assessment of syntactic generalization in neural language models. *arXiv preprint arXiv:2005.03692*, 2020.

Jacob Devlin Ming-Wei Chang Kenton and Lee Kristina Toutanova. Bert: Pre-training of deep bidirectional transformers for language understanding. In *Proceedings of NAACL-HLT*, pages 4171–4186, 2019.

Trenton E. Kriete, David C. Noelle, Jonathan D. Cohen, and Randall C. OâReilly. Indirection and symbol-like processing in the prefrontal cortex and basal ganglia. *Proceedings of the National Academy of Sciences*, 110:16390 – 16395, 2013.

Karol Kurach, Marcin Andrychowicz, and Ilya Sutskever. Neural random-access machines. *arXiv preprint arXiv:1511.06392*, 2015.

Brenden Lake and Marco Baroni. Generalization without systematicity: On the compositional skills of sequence-to-sequence recurrent networks. In *International conference on machine learning*, pages 2873–2882. PMLR, 2018.

Brenden M Lake. Compositional generalization through meta sequence-to-sequence learning. *Advances in neural information processing systems*, 32, 2019.

Hung Le, Truyen Tran, and Svetha Venkatesh. Neural stored-program memory. In *International Conference on Learning Representations*, 2020a. URL `https://openreview.net/forum?id=rkxxA24FDr`.

Hung Le, Truyen Tran, and Svetha Venkatesh. Self-attentive associative memory. In Hal DaumÃ© III and Aarti Singh, editors, *Proceedings of the 37th International Conference on Machine Learning*, volume 119 of *Proceedings of Machine Learning Research*, pages 5682–5691, Virtual, 13–18 Jul 2020b. PMLR.

Yuxuan Li and James McClelland. Systematic generalization and emergent structures in transformers trained on structured tasks. In *NeurIPS '22 Workshop on All Things Attention: Bridging Different Perspectives on Attention*, 2022. URL `https://openreview.net/forum?id=BTNaKmYdQmE`.

Qian Liu, Shengnan An, Jian-Guang Lou, Bei Chen, Zeqi Lin, Yan Gao, Bin Zhou, Nanning Zheng, and Dongmei Zhang. Compositional generalization by learning analytical expressions. *Advances in Neural Information Processing Systems*, 33:11416–11427, 2020.

Minh-Thang Luong, Hieu Pham, and Christopher D Manning. Effective approaches to attention-based neural machine translation. *arXiv preprint arXiv:1508.04025*, 2015.

Benjamin Newman, John Hewitt, Percy Liang, and Christopher D. Manning. The eos decision and length extrapolation. In *BlackBoxNLP@EMNLP*, 2020. URL `https://nlp.stanford.edu/pubs/newman2020extrapolation.pdf`.

Maxwell Nye, Armando Solar-Lezama, Josh Tenenbaum, and Brenden M Lake. Learning compositional rules via neural program synthesis. *Advances in Neural Information Processing Systems*, 33:10832–10842, 2020.

Jing Qian, Hong Wang, Zekun Li, Shiyang Li, and Xifeng Yan. Limitations of language models in arithmetic and symbolic induction. In Anna Rogers, Jordan L. Boyd-Graber, and Naoaki Okazaki, editors, *Proceedings of the 61st Annual Meeting of the Association for Computational Linguistics (Volume 1: Long Papers), ACL 2023, Toronto, Canada, July 9-14, 2023*, pages 9285–9298. Association for Computational Linguistics, 2023. doi: 10.18653/v1/2023.acl-long.516. URL `https://doi.org/10.18653/v1/2023.acl-long.516`.

Pranav Rajpurkar, Jian Zhang, Konstantin Lopyrev, and Percy Liang. Squad: 100,000+ questions for machine comprehension of text. In *Proceedings of the 2016 Conference on Empirical Methods in Natural Language Processing*, pages 2383–2392, 2016.

Jake Russin, Jason Jo, Randall C O'Reilly, and Yoshua Bengio. Compositional generalization in a deep seq2seq model by separating syntax and semantics. *arXiv preprint arXiv:1904.09708*, 2019.

David Saxton, Edward Grefenstette, Felix Hill, and Pushmeet Kohli. Analysing mathematical reasoning abilities of neural models. In *International Conference on Learning Representations*, 2018.

Peter Shaw, Ming-Wei Chang, Panupong Pasupat, and Kristina Toutanova. Compositional generalization and natural language variation: Can a semantic parsing approach handle both? In *Proceedings of the 59th Annual Meeting of the Association for Computational Linguistics and the 11th International Joint Conference on Natural Language Processing (Volume 1: Long Papers)*, pages 922–938, 2021.

Ray J Solomonoff. Algorithmic probability, heuristic programming and agi. In *3d Conference on Artificial General Intelligence (AGI-2010)*, pages 57–63. Atlantis Press, 2010.

Mirac Suzgun, Sebastian Gehrmann, Yonatan Belinkov, and Stuart M Shieber. Memory-augmented recurrent neural networks can learn generalized dyck languages. *arXiv preprint arXiv:1911.03329*, 2019.

Xiaojuan Tang, Zilong Zheng, Jiaqi Li, Fanxu Meng, Song-Chun Zhu, Yitao Liang, and Muhan Zhang. Large language models are in-context semantic reasoners rather than symbolic reasoners. *arXiv preprint arXiv:2305.14825*, 2023.

Ashish Vaswani, Noam Shazeer, Niki Parmar, Jakob Uszkoreit, Llion Jones, Aidan N Gomez, Łukasz Kaiser, and Illia Polosukhin. Attention is all you need. *Advances in neural information processing systems*, 30, 2017.

Oriol Vinyals, Meire Fortunato, and Navdeep Jaitly. Pointer networks. *Advances in neural information processing systems*, 28, 2015.

John Von Neumann. First draft of a report on the edvac. *IEEE Annals of the History of Computing*, 15(4):27–75, 1993.

Taylor Whittington Webb, Ishan Sinha, and Jonathan Cohen. Emergent symbols through binding in external memory. In *International Conference on Learning Representations*, 2020.

Jason Weston, Antoine Bordes, Sumit Chopra, Alexander M Rush, Bart Van Merriënboer, Armand Joulin, and Tomas Mikolov. Towards ai-complete question answering: A set of prerequisite toy tasks. *arXiv preprint arXiv:1502.05698*, 2015.

Bo Wu, Haoyu Qin, Alireza Zareian, Carl Vondrick, and Shih-Fu Chang. Analogical reasoning for visually grounded language acquisition. *arXiv preprint arXiv:2007.11668*, 2020.

Greg Yang. Lie access neural turing machine. *arXiv preprint arXiv:1602.08671*, 2016.

Xiang Yu, Ngoc Thang Vu, and Jonas Kuhn. Learning the dyck language with attention-based seq2seq models. In *Proceedings of the 2019 ACL Workshop BlackboxNLP: Analyzing and Interpreting Neural Networks for NLP*, pages 138–146, 2019.

Biao Zhang, Ivan Titov, and Rico Sennrich. Improving deep transformer with depth-scaled initialization and merged attention. In *Proceedings of the 2019 Conference on Empirical Methods in Natural Language Processing and the 9th International Joint Conference on Natural Language Processing (EMNLP-IJCNLP)*, pages 898–909, 2019.

Appendix

A More Discussion on Related Works

The proposed address attention in our paper is comparable to two known mechanisms: (1) location-based attention (Luong et al., 2015; Dubois et al., 2020) and (2) memory shifting (Graves et al., 2014; Yang, 2016). The former uses neural networks to produce attention weights to the memory/sequence, which cannot help when the memory grows during inference since the networks never learn to generate weights for the additional slots. Inspired by Turing Machine, the latter aims to shift the current attention weight associated with a memory slot to the next or previous slot. Shifting-like operations can handle any sequence length. However, it cannot simulate complicated manipulation rules. Unlike our `PU` design which obeys § 1's principle **II**, the attention weight and the network trained to shift it depend on the memory content `M`. That is detrimental to generalization since new content can disturb both the attention weight and the shifting network as the memory grows.

Another line of works tackles systematic generalization through meta-learning training (Lake, 2019), while our method employs standard supervised training. These approaches are complementary, with our method concentrating on enhancing model architecture rather than training procedures, making it applicable in diverse settings beyond SCAN tasks. Additionally, the study by Hu et al. (2020) addresses syntactic generalization (Hu et al., 2020), a different problem compared to our paper, which emphasizes length extrapolation across various benchmarks. Notably, our paper considers similar baselines, such as LSTM and Transformer, as those examined in the referenced papers. There are other lines of research targeting reasoning and generalization using image input(Wu et al., 2020; Eisermann et al., 2021). They are outside the scope of our paper, which specifically addresses generalization for longer sequences of text or discrete inputs

Our address bank and physical pointers can be viewed as some form of positional encoding. However, we do not use simple projections or embeddings to force the attention to be position-only. Instead, we aim to learn a series of transformations that simulate the position-based symbolic rules. At each time step, a new pointer ("position") is dynamically generated that reflects the manipulation rule required by the task (e.g. move to the next location), which is unlike the positional encoding approaches such as RPE (Dai et al., 2019) which aims to provide the model with information on the relative position or distance of the timesteps. We summarise the difference between our method and Transformer in Table 3.

B More Discussion on Base Address Sampling Mechanism

We provide a simple example to illustrate how base address sampling help in generalization. Assume the training sequence length is 10, and the desired manipulation is $p' = p + 1$ (copy task). Assume the possible address range is $0, 1, ..., 19$, which is bigger than any sequence length. If $p_B = 0$, the training address bank contains addresses: $0, 1, ...8, 9$. Without base address sampling, the model always sees the training address bank of $0, 1, ...8, 9$ and thus can only learn manipulating function for $0 \leq p \leq 9$, thereby failing when testing address bank includes addresses larger than 9.

Thanks to base address sampling, at some point of training, $p_B = 10$, the training address bank is $10, 11, ...13, 19$. The manipulating function sees $p > 9$ and can learn to transform $p' = p + 1$ for $p > 9$, e.g., transform $p = 10 \rightarrow p' = 11$. The learning happens because the pointer's value ($^*p$) is used to predict the output sequence. The task loss will reward $^*p$ that follows the rule, and update the Pointer Unit such that it transforms the p following the rule to minimize the loss. During testing, the input length can be 12, we set $p_B = 0$ and the address bank is $0, 1, ..., 10, 11$. The learned manipulation can still be applied to new locations 10th, and 11th.

We can prove that the complexity of exposing all addresses to the model is practically small compared to the normal training. Assume the training input sequence length is L, and the number of possible addresses is L_{max}. Here, L_{max} indicates the possible testing length that the model can handle. When $L_{max} \rightarrow \infty$, the expected number of samples required for exposing all addresses is $O(n \log n)$ where $n = L_{max}/L$ (we can formulate this problem as

Difference	Transformer	PANM (Our)
Key Generation	Keys are computed based on input data. Hence, when meeting novel data during testing, Transformer will observe novel keys, and cannot work properly.	The keys in our approach are generated as fixed numbers, specifically physical memory addresses. These keys are entirely separate from the data.
Extendable to Longer Sequences	The dimension of attention weights varies with input length, making arithmetic transformations on these attention weights infeasible as the sequence length increases.	The fixed nature of our physical addresses allows our pointers to be easily manipulated and extendable to longer sequences.
Symbol Processing Advantages	The use of attention weights as implicit pointers may lack the explicitness needed for effective symbol processing.	Using physical addresses as keys in our approach is crucial for symbol processing as it explicitly allows pointer assignment, dereference, and arithmetic operations.
Physical Address vs Positional Encoding	Positional encoding can be generated independently from data. However, they are not separated from the input data as our physical addresses. There is no explicit mechanism in Transformer to attend only to these positional encodings or to transform pointers to point to these positional encodings from one step to another.	Our physical addresses are detached from the data, supporting the transformation of pointers through timesteps and isolating pointer manipulation from the input.

Table 3: PANM vs Transformer

Coupon collector's problem). For example, in even an extreme address range of $L_{max} = 10^6$ (in practice we rarely need that big range) to train input sequences of length 10, we only need to sample $10^5 \log 10^5$ sequences, which is often smaller than the size of the training datasets. Empirically, in our experiments, we always train our method with the same number of batch size and training steps as other baselines to ensure a fair comparison, and we realize that it is always possible to expose all the addresses to our model during training.

C More Discussion on Model and Architecture

We can see that it is critical to have $H^a \geq 2$ and $p_B, p_E \in \left\{p^a_{0,h}\right\}_{h=1}^{H^a}$ to achieve generalization using pointer arithmetic. In other words, if $p_B, p_E \notin \left\{p^a_{0,h}\right\}_{h=1}^{H^a}$, we can always find a task to make PANM fail to generalize. For example, if $p_E \notin \left\{p^a_{0,h}\right\}_{h=1}^{H^a}$, PANM cannot generalize in Reverse task. To see that, without loss of generality, we assume PANM only learn to produce the last token at address p_E using information from some initial addresses $p' \in \left\{p^a_{0,h}\right\}_{h=1}^{H^a}$ such that $p' \neq p_E$. During training, the learned pointer arithmetic to perform Reverse at the first step of the decoding to produce value y_1 can only be a function of p': $y_1 = {}^*p_E =^* f(p')$, that is, $p_E = f(p')$. During testing, p_E can receive arbitrary value, so for whatever learned f, we can always find a test sequence such that $p_E \neq f(p')\ \forall f$ because $p_E \neq p'$. A similar argument can be used for p_B and Copy task.

In the main manuscript, we only experiment with 1 Mode-2 pointer ($H^c = 1$). If $H^c = 0$, obviously PANM will fail in tasks such as ID Sort. Using more H^c and H^a can still be beneficial in exchange for slower computation (see Appendix D.5). In all experiments, we use 256-dimensional GRUs for the `PU` and `Ctrl`. The encoder and decoder (to stack the Controller on) can vary across tasks. The general plug-and-play framework is illustrated in Fig. 3. We also summarize operations of our model in Algo. 1.

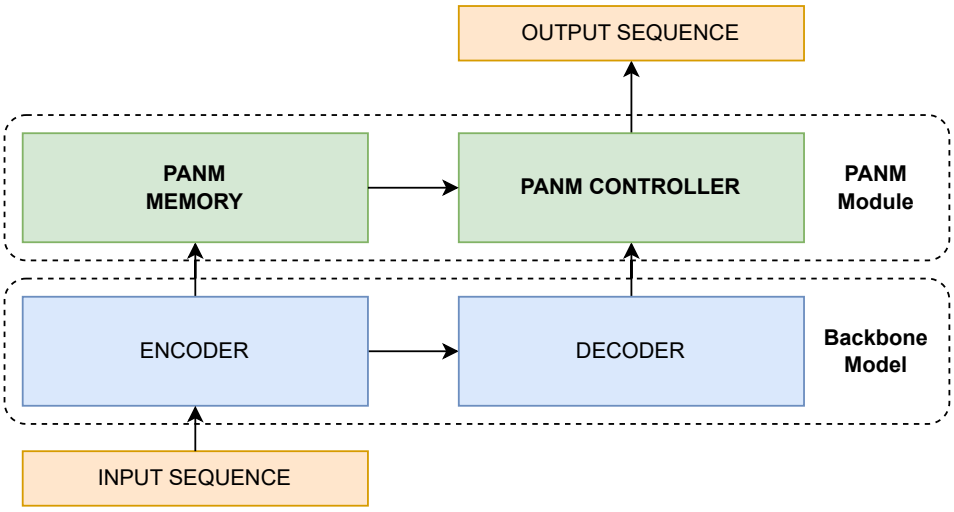

Figure 3: PANM as a plug-and-play architecture. The encoder and decoder can be any model (LSTM, Transformer or BERT). PANM Controller can be used as the last layer of the Decoder to access the memory during decoding. To reduce the number of parameters of the augmented architecture, the decoder's number of layers can be decreased.

D Experimental Details

All the datasets and public codebases use Apache or MIT License. We trained all the models using a single GPU Tesla V100-SXM2. The running time of PANM depends on the `Encoder` and tasks. Overall, with 2 Mode-1 pointers and 1 Mode-2 pointer, PANM's speed will be 70-80% compared to the backbone model. For example, in Copy task, PANM's speed is 15 iterations/s while LSTM's is 20 iterations/s. If PANM uses Transformer Encoder, its speed is 77 iterations/s while Transformer's is 90 iterations/s.

Baseline Choice Although our baselines are classic, they are still very strong baselines in our studied tasks. For example, in our algorithmic reasoning, LSTM with attention or Pointer Networks are still dominant baselines, outperforming the more recent Transformer. In Dyck recognition, stack-based models are still SOTA because their inductive bias is suitable for the task. Experiments in Sec. 3 adopt (Universal) Transformer+RPE, which is a recent and strong Transformer variant focusing on generalization. There are also other sophisticated methods focusing generalization (Webb et al., 2020).

In our experiments, PANM is ensured to have similar model size as the baselines and often built on top of similar backbones for fair comparison. We believe it is still important to improve fundamental baselines such as Transformers or LSTM because they are the building blocks of many practical applications including recent Large Language Models (LLMs). In this paper, we prove the improvement of these fundamental blocks, and in future works, we will extend our ideas to more advanced backbones such as LLMs.

Algorithm 1 PANM training. To simplify, we assume the batch size and number of pointer heads of one.

Input: A dataset of sequence pairs $D = \{X_i, Y_i\}_{i=1}^{N_{data}}$, initial Φ containing the parameters of the $\texttt{Encoder}_\theta$, Pointer Unit $\texttt{PU}_\varphi$ and Controller $\texttt{Ctrl}_\lambda$, b representing the number of bits of the address space, L_{dec} being the maximum number of decoding steps, and function l measuing the length of a sequence.

Ouput: Φ^*, trained parameters.

for $\{X_i, Y_i\} \sim D$ **do**
  `/* Construct the memory */`
  $\texttt{M} = \texttt{Encoder}_\theta(X_i)$
  `/* Sample base address. During testing,` p_B `can be set to 0 */`
  $p_B \sim \text{Uniform}\left(\{0,1\}^b\right)$
  `/* Generate the address */`
  for $j = 0, 1, ..., l(\texttt{M}) - 1$ **do**
    $\texttt{A}[j] = (p_B + j) \bmod 2^b$
  end
  `/* Decode with pointers */`
  for $t = 0, 1, ..., L_{dec}$ **do**
    Use $\texttt{PU}_\varphi$ and $\texttt{A}$ to compute p_t^a using Eq. 1
    Use $\texttt{M}$ and p_t^a to compute pointer values ${}^*p_t^a$ (Mode 1) and ${}^*p_t^c$ (Mode 2) (see §2.3.2)
    Use $\texttt{Ctr}_\lambda$ and pointer values to compute $p_\Phi(y_t|X_i, z_t)$ (see §2.3.3)
    $\hat{y}_t^i = \text{argmax}_{y_t}\ p_\Phi(y_t|X_i, z_t)$
    if $\hat{y}_t^i$ *is eos* **then**
      break
    end
  end
  `/* Compute cross-entropy loss */`
  $\mathcal{L} = -\sum_t \log p_\Phi(y_t = Y_i[t]|X_i, y_{t-}^i)$
  Use $\mathcal{L}$ to update Φ through backpropagation
end

D.1 Algorithmic Reasoning

We first give the details of the content-based tasks below.

In **Dynamic Recall**, an arbitrary input token is chosen as the query and is added to the end of the input sequence. Depending on the length of the input, a.k.a, odd or even, the first target token will be on the left or right of the query, following its succeeding tokens in the input. This task requires both content matching (find query token in the input sequence) and position-based access (shift left or right).

In **Priority Sort**, each input token is associated with a priority score sampled from the standard normal distribution. The target output will be tokens from the input sequence sorted ascending by their the score. This task can be solved in many ways and likely needs complicated symbol processing such as looping through items in the sequence and comparing the score of tokens.

Finally, in **ID Sort**, each input token is augmented with an id feature vector sampled from standard multivariate normal distribution such that every 2 tokens share one id. For example, with input x_1, x_2, x_3, x_4, x_1 and x_4 may share one id while x_2 and x_3 shares another id. The pairing is chosen randomly. The output token at position i-th will be the input token that share id with the i-th input token. The correct output for the earlier example is x_4, x_3, x_2, x_1. This task is specifically designed to test the ability to learn Mode 2 pointer-based memory access.

In this task, we implement the baselines such as LSTM, attention models and Transformer using Pytorch library. The hidden state dimension for these models are set to 512, which results in around 1-3 millions parameters. We tuned the number of layers of the encoder/decoder for these baselines in Copy task, and realized that 1-layer gave the best

performance. For NTM and DNC, we use public repositories[1] with default controller's hidden state of 256 dimensions and 128-slot external memory, which results in around 1.2 millions parameters. We use the ESBN's author codebase [2] with default parameter setting, resulting in ≈1.2 million parameters. For PtrNet, since we do not use token index as the training label, we produce the predicted token by performing weighted sum the input tokens using the PtrNet's attention weights. PtrNet's hyperparameters are the same as attention models. We could not find the authors' code for Neural Stack and NRAM so we implemented them and tuned hyperparameters for the Copy task at length L such that the model sizes are about 1.1 million parameters. In this task PANM uses LSTM with hidden state of 256 as the `Encoder` and does not stack the Controller on any decoder models, resulting in ≈1.1 million parameters.

In this experiment, all the models are trained without teacher forcing as in Graves et al. (2014), i.e, the input to the decoder is zero ($z_t = 0$). The detailed average accuracy (mean ± std.) of each method together with the actual length of each testing mode are reported in Tables 5-10.

Overall, PANM observes significant improvement ranging from 10-20% on each task. We note that when compared with individual baselines, the improvement is much higher. Consider Copy as an example (Fig. 2a), PANM outperforms the worst baseline Transformer by around 60% at $2(L+1)$ and 30% at $4(L+1)$, respectively. As stated earlier that our tasks are challenging, thus, originally strong baselines such as NTM, DNC, and Neural Stack do not generalize well at extreme lengths, especially in ID Sort. ID Sort is trickier than content-free tasks, making some baselines fail at length L even though it is in the training data. The best other model in this case is Content Attention, which clearly underperforms our PANM from few % to 50% (Fig. 2b). Without curriculum learning and under the 10-class prediction setting, methods that use implicit pointers, such as PtrNet, NRAM, and ESBN, demonstrate mediocre performance on average when compared to PANM. Furthermore, PANM also outperforms in length-dependent tasks (Mix, D. Recall), indicating that it can track the sequence length in extrapolation. We hypothesize that PANM's content–free pointer generation mechanism to simulate list iteration makes it possible.

In Copy, only Mode-1 access is needed. As decoding step t increases, Pointer Unit generates p_t^a following the increment of the addresses as expected. That said, for several steps, the address attention is not sharp, showing other addresses pointed by the pointer, which is not surprising since we use soft attention and it is hard for a neural network to learn the exact rule: $p_{t+1}^a = p_t^a + 1$. This problem gets worse as test length increases as the error accumulates, especially when the same token can appear many times, which confuses the model. This explains why PANM's performance drops clearly in the hardest case $8(L+1)$. Yet, it is still significantly better than others whose results are near random prediction.

D.2 Dyck Language Recognition

In this task, we adopt the SRNN code from Suzgun et al. (2019)[3] using the default parameters. As explained in the main text, this task is auto-regression, hence, $z_t = \hat{y}_{t-1}$. PANM adopts SRNN (an auto-regressive model) as the encoder and does not stack the Controller on any decoder models. The result is visualized in Fig. 4 (left).

D.3 Conpositional Learning

In this task, we adopt the code from Csordás et al. (2021)[4] using the default parameters. When using Transformer Encoder, we need to have Transformer-like decoder to align the token representation of the encoding and decoding phases. As such, in SCAN, we utilize the 3-layer Transformer decoder, replace its last layer by the Controller. Formally, z_t in Eq. 3 becomes Decoder(y_{t-}) where the Decoder is a 2-layer Transformer. In Mathematics reasoning task, we use similar integration except that the Encoder is Transformer with

[1] `https://github.com/thaihungle/SAM`

[2] `https://github.com/taylorwwebb/emergent_symbols`

[3] `https://github.com/suzgunmirac/marnns`

[4] `https://github.com/RobertCsordas/transformer_generalization`

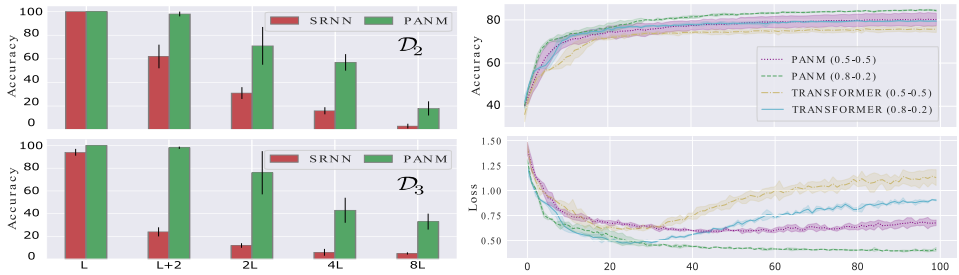

Figure 4: Dyck (Left): mean ± std. accuracy over 5 runs with different testing lengths. bAbI QA (Right): mean ± std. testing accuracy and cross-entropy loss across 100 training epochs over 5 runs.

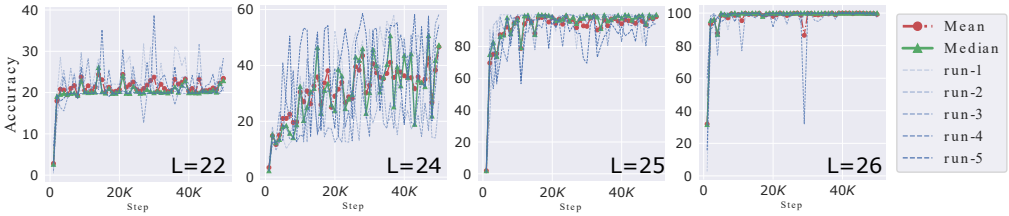

Figure 5: SCAN: PANM's exemplar learning curves.

relative positional encoding (TRM + RPE). By reducing the number of decoding layer, we ensure PANM's hyperparameter number equivalent to that of the Transformer baseline (12M). All models are trained with teacher forcing as in Csordás et al. (2021).

SCAN The training size is 16990 and the test size is 3920. SCAN is a well-known and standard benchmark for testing compositional learning and generalization in sequential models. One property of this dataset is that a new length often contains new rules that must be captured by the model to ensure generalization, and thus, if the model fails to learn a hidden rule, its performance may drop significantly from one length split to another. Fig. 5 illustrates PANM's testing accuracy curves when $L = 22, 24, 25, 26$. Other learning curves for $L > 26$ looks similar to $L = 26$ where PANM easily solves the task perfectly.

Mathematical Problems Table 11 reports the accuracy with mean and standard deviation. Here, we augment TRM and TRM+RPE with PANM. Both shows improvement, especially for TRM+RPE, indicating that PANM is compatible with other methods designed to improve generalization in Transformer.

D.4 Other NLP Tasks

The bAbI dataset consists of 20 synthetic tasks that evaluate various reasoning skills. To prepare the data for each task, we combine train/valid/test into a single set and sort it by length and split it into training and testing sets, as described in the main text. We train the models jointly on all 20 tasks and measure the accuracy of their answers, which are considered correct only if they match the ground truth answer perfectly. The training/evaluation follows exactly the standard protocol presented in (Le et al., 2020b). The Transformer used here has 8 heads, 3 layers of encoding, 3 layers of decoding, and hidden dimensions of 512. PANM uses the same Transformer backbone except that the decoder has 2 layers to make the model size equivalent. We run each model 5 times to report the mean and standard deviation as in Fig. 4 (right). Table 12 reports the detailed numbers.

The SQUAD dataset contains more than 100K realistic context/question-answer pairs. Again, we combine train/test into a single set and sort it by length and split into new train/test sets. Following Kenton and Toutanova (2019), we use BERT model (`https://huggingface.co/bert-base-uncased`) to predict the start and end location of the answer, and finetune the model with the same setting (e.g., 3 epochs with a learning rate of

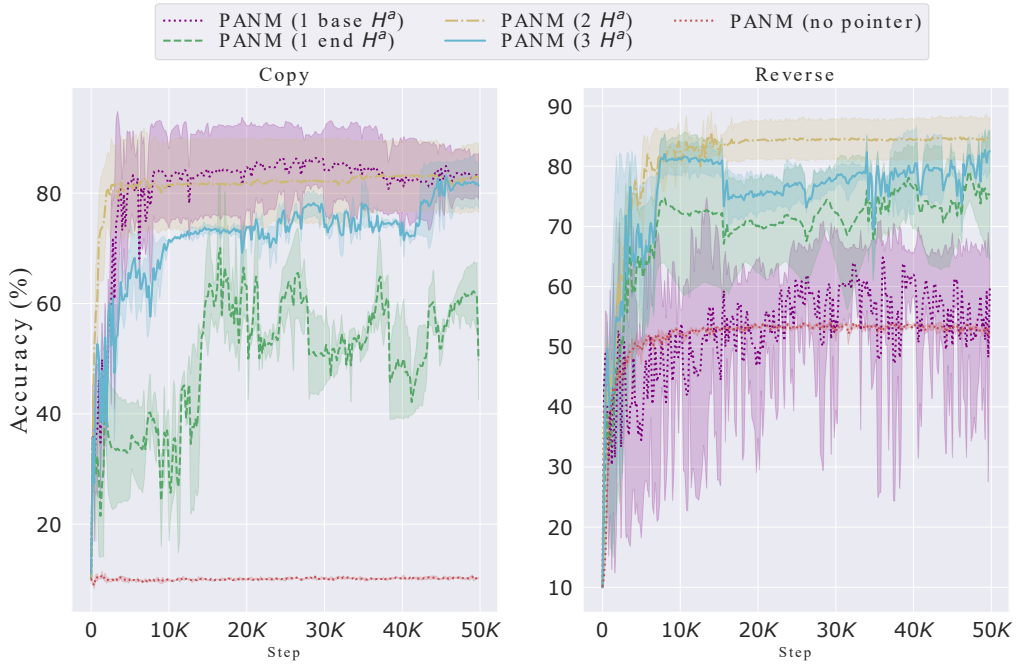

Figure 6: Testing accuracy (mean ± std.) at 2(L+1) length over training steps. Different configurations of Mode-1 pointers are trained and evaluated 5 times.

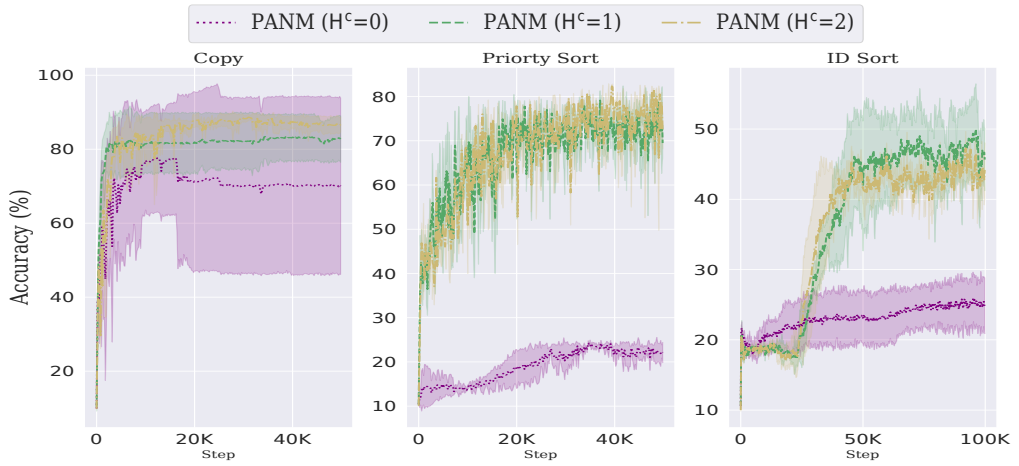

Figure 7: Testing accuracy (mean ± std.) at 2(L+1) length over training steps. Different configurations of Mode-2 pointers are trained and evaluated 5 times.

5e-5) except that our batch size is 16 to fit with our GPU. PANM appends the Controller to BERT to predict the start and end. Both BERT and PANM have around 114 million parameters. Table 13 reports the detailed numbers.

D.5 Additional Experiments

Pointer Hyperparameters In this section, we confirm the logic presented in Appendix C by performing experiments that involve varying the number and type of pointers.

Mode-1 Pointers We test the PANM version in § 3.1 with $H^a = 0, 1, 2, 3$ on Copy, Reverse. We do not use Mode-2 pointer here to avoid confusion ($H^c = 0$). Fig. 6 plots the testing accuracy over training time. As $H^a = 0$, there is no pointer information for the Controller,

PANM should be equivalent to an GRU and fail to generalize. As $H^a = 1$, the only pointer is initialized either with the base or end address. As shown in Fig., PANM cannot generalize in both Copy and Reverse tasks with single Mode-1 pointer, which is proved in Appendix C. In the case$H^a = 3$, we initialize them with the base, end and middle addresses. We observe that increasing H^a to 3 slightly reduces the performance in these tasks. We speculate that too many Mode-1 pointers make the learning harder; in particular, learning to manipulate the third pointer may interfere with that of the first or second pointer, which are more important in these tasks. Generally, most tasks only require list iterations from the head to the tail or vice versa. Hence, we keep $H^a = 2$ in all experiments to save the computation cost.

Mode-2 Pointers We fix $H^a = 2$, and vary $H^c = 0, 1, 2$ on Copy, Priority Sort, ID Sort. As shown in Fig. 7, without Mode-2 pointers ($H^c = 0$), generalization in Priority Sort and ID Sort is reduced significantly by 50% and 30%, respectively because these tasks focus more on the content of the input sequence and often demand comparing the content of different tokens. Interestingly, a content-free task like Copy also suffers from performance drop if there is no Mode-2 pointer. Specifically, we find out that for 2/5 runs, the model converges to a suboptimal solution, leading to high variance and slightly lower mean accuracy. Perhaps, Mode-2 pointer allows the decoder to access the input instantly (like content-based attention), avoid forgetting, and thus, improve the prediction as the sequence is longer. Having more Mode-2 pointers generally improves the generalization in Copy and Priority Sort, yet the gain is small for $H^c = 2$, or even negative in ID Sort. Therefore, we trade-off performance with computing efficiency by setting $H^c = 1$ in our experiments.

D.6 Failures of Chat-GPT in Our Tasks

Large Language Models (LLMs), especially Chat-GPT, have shown remarkable results in reasoning and generalization. Directly comparing Chat-GPT with other models used in our experiments would be unfair because Chat-GPT was not directly trained with our datasets and it has much more parameters than our model. Therefore, in this section, we merely use Chat-GPT as a tool to verify that our chosen tasks, despite being simple, are non-trivial. The evaluated tasks are algorithmic reasoning and SCAN. We do not examine Dyck recognition because the output encoding is complicated to represent in text. Other datasets are more common and likely to be used for training Chat-GPT, thus, are not suitable for generalization test. For example, in Mathematics task, if we ask Chat-GPT the question from the data `What is the hundreds digit of 31253`?, it provide the correct answer (`2`). However, slightly modifying the question to ensure it does not appear in the training and testing set will successfully fool Chat-GPT:

- Example 1:
  - Prompt: What is the hundreds digit of 312537?
  - Chat-GPT answer: The hundreds digit of the number 312537 is 2.
- Example 2:
  - Prompt: What is the hundreds digit of 319253?
  - Chat-GPT answer: The hundreds digit of the number 319253 is 9.

We use Open AI's Chat-GPT 3.5 version September and evaluate the model on our data using few-shot example prompts, following the format:

Examples:
input $x_1^1, x_2^1, ...$ output $y_1^1, y_2^1, ...$
input $x_1^2, x_2^2, ...$ output $y_1^2, y_2^2, ...$
...
Question:
input $x_1, x_2, ...$ output

Algorithmic Reasoning To ensure that Chat-GPT does not memorize the output answer from its vast training data, we use non-digit symbols: ~!@#$%^&*(as 10 tokens of the

Task	Chat-GPT	Failure example			PANM
		Input	Chat-GPT Output	True Output	
Copy	100%	N/A			84%
Reverse	69%	$%&&$%^@%#	%#^@^%$&&%$	#%@^%$&&%$	84%
Mix	42%	$%&&$%^@%#	%#^&&$%$@%&	$%$&$%$@$#	98%
Dynamic Recall	14%	$(&&$#^@%# %	$	@	45%

Table 4: Failure of Chat-GPT on algorithmic reasoning test cases of length $2L$. Token-level accuracy is reported. We do not test Chat-GPT on Priority and ID sort because they have complicated token representations. PANM results cannot be directly compared, and shown for reference only.

Copy Task	9(L)	10(L+1)	20((L+1)*2)	40((L+1)*4)	80((L+1)*8)
LSTM	100±0	47±0	11±0	10±0	10±0
Location Attention	100±0	93±2	51±5	28±4	20±1
Content Attention	100±0	92±1	53±0	33±0	22±0
Hybrid Attention	100±0	91±1	50±1	23±3	13±0
Transformer	100±0	20±1	16±0	13±0	11±0
NTM	100±0	74±4	13±2	11±0	11±0
DNC	100±0	54±2	11±1	11±0	11±0
Neural Stack	100±0	90±4	47±2	29±0	17±0
PtrNet	100±0	90±2	52±1	32±1	20±0
NRAM	100±0	81±3	15±2	11±0	11±1
ESBN	100±0	92±0	34±0	11±0	11±0
PANM	**100±0**	**100±0**	**84±1**	**52±1**	**36±1**

Table 5: Copy: accuracy (mean ± std. over 5 runs)

datasets. For each task, we sample 20 training examples of length $L = 5$ to build the in-context examples, and test on 1 longer sequence of length $2L = 10$. We conduct 20 trials and report the average test accuracy. Table 4 summaries the evaluation results. Overall, except for Copy task where Chat-GPT shows excellent generalization, other tasks are very hard for Chat-GPT, indicating that the length extrapolation problem still poses a big challenge to today AI techniques.

SCAN In this task, we sample 20 examples in the L-cutoff=40 split set (easiest) as in-context learning examples and evaluate on 10 unseen sequences. Chat-GPT totally failed in this task. When testing on the similar length or longer length as the examples, Chat-GPT cannot produce any exact match results (exact match accuracy=0). Below are some failure examples:

- IN: walk and turn opposite right OUT:
  - Chat-GPT output: I_TURN_RIGHT I_TURN_RIGHT I_WALK
  - True output: I_WALK I_TURN_RIGHT I_TURN_RIGHT
- IN: run around left twice and run around right OUT:
  - Chat-GPT output: I_RUN I_TURN_LEFT I_RUN I_TURN_LEFT I_RUN I_TURN_RIGHT I_RUN
  - True output: I_TURN_LEFT I_RUN I_TURN_LEFT I_RUN I_TURN_LEFT I_RUN I_TURN_LEFT I_RUN I_TURN_LEFT I_RUN I_TURN_LEFT I_RUN I_TURN_LEFT I_RUN I_TURN_LEFT I_RUN I_TURN_LEFT I_RUN I_TURN_RIGHT I_RUN I_TURN_RIGHT I_RUN I_TURN_RIGHT I_RUN I_TURN_RIGHT I_RUN

Reverse Task	9(L)	10(L+1)	20((L+1)*2)	40((L+1)*4)	80((L+1)*8)
LSTM	100±0	96±0	53±0	33±0	22±0
Location Attention	100±0	26±3	18±1	14±0	12±0
Content Attention	100±0	81±25	38±11	23±4	16±2
Hybrid Attention	100±0	98±1	50±7	24±2	15±1
Transformer	100±0	18±0	15±3	13±1	11±0
NTM	100±0	95±7	65±27	26±13	13±1
DNC	100±0	93±3	60±18	23±6	12±1
Neural Stack	100±0	96±1	64±4	35±3	19±1
PtrNet	100±0	77±5	32±4	22±1	12±0
NRAM	100±0	96±1	60±3	33±2	15±2
ESBN	99±0	95±0	14±2	11±0	10±0
PANM	**100±0**	**100±0**	**84±3**	**51±1**	**33±1**

Table 6: Reverse: accuracy (mean ± std. over 5 runs)

Mix Task	9(L)	10(L+1)	20((L+1)*2)	40((L+1)*4)	80((L+1)*8)
LSTM	100±0	96±0	53±0	33±0	22±0
Location Attention	100±0	92±10	56±1	45±0	30±6
Content Attention	100±0	61±8	57±1	14±0	12±0
Hybrid Attention	100±0	98±1	56±3	34±0	23±6
Transformer	100±0	18±0	15±3	13±1	11±0
NTM	100±0	95±7	65±27	26±13	13±1
DNC	100±0	91±4	58±9	19±3	11±1
Neural Stack	100±0	87±3	50±5	14±2	11±0
PtrNet	100±0	59±3	51±3	13±1	11±0
NRAM	99±0	82±7	48±6	17±4	10±1
ESBN	99±0	95±0	14±2	11±0	10±0
PANM	**100±0**	**100±0**	**98±1**	**54±0**	**54±1**

Table 7: Mix: accuracy (mean ± std. over 5 runs)

Drecall Task	9(L)	10(L+1)	20((L+1)*2)	40((L+1)*4)	80((L+1)*8)
LSTM	85±7	74±16	21±2	12±1	11±0
Location Attention	88±1	82±1	30±3	19±2	13±0
Content Attention	88±2	84±0	27±3	17±1	13±1
Hybrid Attention	69±25	66±24	28±4	19±2	13±1
Transformer	33±1	32±0	22±0	14±1	12±1
NTM	86±3	72±8	22±1	15±0	12±0
DNC	89±0	83±1	22±1	14±2	11±0
Neural Stack	85±4	76±2	23±1	15±1	13±1
PtrNet	65±14	48±7	25±6	14±1	12±1
NRAM	61±6	59±4	21±4	13±2	11±1
ESBN	90±1	86±1	22±3	11±1	10±0
PANM	**92±0**	**89±0**	**45±1**	**22±0**	**16±0**

Table 8: Drecall: accuracy (mean ± std. over 5 runs)

PSort Task	10(L)	11(L+1)	21((L+1)*2)	41((L+1)*4)	81((L+1)*8)
LSTM	87±2	83±2	28±3	16±1	12±1
Location Attention	69±3	66±3	45±1	27±2	20±2
Content Attention	**97±0**	96±0	57±6	30±7	22±5
Hybrid Attention	85±3	81±1	33±1	25±2	23±3
Transformer	71±9	48±8	21±3	16±4	14±4
NTM	96±2	95±3	34±18	12±1	10±0
DNC	95±0	92±2	29±7	11±1	10±0
Neural Stack	92±2	79±2	32±3	13±2	11±1
PtrNet	77±2	71±2	43±2	24±1	19±1
NRAM	82±3	80±2	51±2	25±1	13±1
ESBN	26±4	24±4	13±2	11±1	10±0
PANM	**97±0**	**97±1**	**86±2**	**32±7**	**27±4**

Table 9: PSort: accuracy (mean ± std. over 5 runs)

ID Sort Task	10(L)	11(L+1)	21((L+1)*2)	41((L+1)*4)	81((L+1)*8)
LSTM	48±10	40±5	20±1	13±1	11±1
Location Attention	34±1	32±1	20±0	14±0	12±0
Content Attention	98±1	56±1	28±2	16±0	12±0
Hybrid Attention	32±1	31±1	19±1	14±0	12±0
Transformer	34±2	29±0	19±0	15±0	12±0
NTM	40±23	32±17	16±4	12±2	11±0
DNC	35±1	36±1	23±2	17±2	13±0
Neural Stack	33±3	32±1	19±1	13±1	12±0
PtrNet	27±1	24±1	15±0	12±1	11±0
NRAM	31±2	29±1	14±0	12±0	11±0
ESBN	47±18	42±12	18±0	12±0	10±0
PANM	**100±0**	**100±0**	**56±2**	**25±0**	**15±0**

Table 10: ID Sort: accuracy (mean ± std. over 5 runs)

Task	`add_or_sub`	`place_value`
U. TRM+ RPE♣	**0.97 ± 0.01**	0.75 ± 0.10
TRM + RPE♣	0.91 ± 0.03	-
TRM + RPE♢	0.91 ± 0.04	0 ± 0
TRM♣	0.89 ± 0.01	0.12 ± 0.07
TRM♢	0.86 ± 0.01	0.05+0.05
U. TRM♣	0.94 ± 0.01	0.20 ± 0.02
PANM TRM base (Ours)	0.91 ± 0.01	0.15 ± 0.02
PANM TRM + RPE base (Ours)	**0.97 ± 0.02**	**0.86 ± 0.05**

Table 11: Mathematics: mean ± std accuracy over 5 runs. ♣ are numbers from Csordás et al. (2021). ♢ is our rerun to confirm the results, which, in some cases, could not match the reported numbers. - means training crash reported in the original papers. We run PANM using the authors' codebase.

Model	Split	
	0.8-0.2	0.5-0.5
Transformer	0.79 ± 0.01	0.76 ± 0.01
U. TRM+ RPE	0.80 ± 0.02	0.75 ± 0.01
PANM (Ours)	**0.85 ± 0.02**	**0.81 ± 0.03**

Table 12: bAbI QA: Testing accuracy (mean ± std.) over 5 runs.

Model	Split			
	0.8-0.2		0.5-0.5	
	F1	EM	F1	EM
BERT	0.77	0.64	0.73	0.59
PANM (Ours)	**0.78**	**0.65**	**0.76**	**0.61**

Table 13: SQUAD 1.1: Testing accuracy after 3 epoch fine-tuning. F1 score and exact match (EM) follows the standard evaluation in (Kenton and Toutanova, 2019).

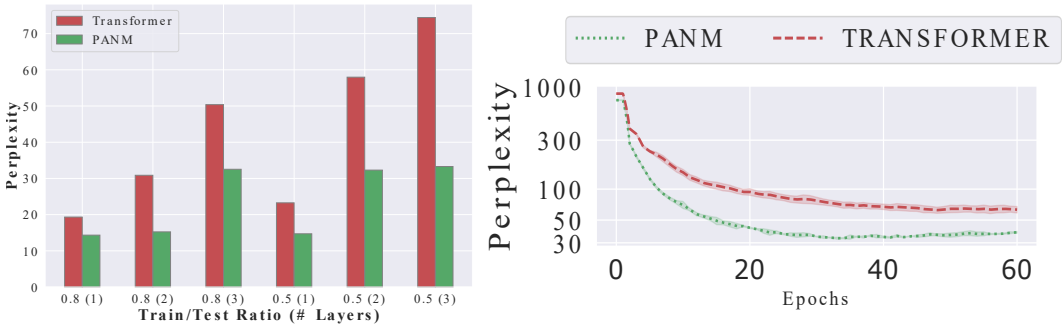

Figure 8: Additional results on machine translation task: Perplexity on Multi30K dataset (the lower the better). We sort the sequences in the data by length and create 2 settings using train/test split of 0.8 and 0.5, respectively. The baselines are Transformer and PANM. **Left:** The best test perplexity over 2 settings for different number of Transformer's layers (1 to 3 layers). **Right:** an example of testing perplexity curves over training epochs for the case of 0.5 train/test split (2 layers) where we run 3 times and report the mean±std. The y-axis is visualized using log scale.